3D Finite Element Modeling of Aircraft Gear Interaction with Cement Concrete Pavement

G. Bonin[1] (guido.bonin@uniroma1.it), F. M. Fiordoliva*[2] (frafiord@mclink.it),
G. Loprencipe[3] (giuseppe.loprencipe@uniroma1.it), A. Ranzo[4] (alessandro.ranzo@uniroma1.it)
Dipartimento di Idraulica, Trasporti e Strade - Università di Roma "La Sapienza", Facoltà di Ingegneria
Via Eudossiana, 18, 00184 Rome, Italy

ABSTRACT

Computational mechanics applied to dynamic impact/interaction problems is nowadays possible. This approach can be used to let the gear and pavement interact in a more complex and realistic way; the FE analysis evaluates either the contact forces and the stresses on the pavement and aircraft gear. This paper describes the development of a 3D Finite Element Model of a cement concrete pavement/joint system and an Airbus 300 gear. The code used to perform all the analysis was LS-DYNA v.950d, a nonlinear explicit Finite Element Analysis code.

In order to examine the effects of the joint bump height and aircraft speed, two different pavement models were used, with and without dowels, running a total of 16+16 simulations (4 different speed, 4 different bump heights for each model). The doweled joint model has been used to evaluate the joint Load Transfer Efficiency, the non-doweled model results have been compared to the values calculated using the Westergaard's theory.

KEYWORDS

Rigid pavement, finite element model, joint, dowel bars, aircraft gear.

---

[1] Ph.D Student
[2] Engineer
[3] Researcher
[4] Professor

INTRODUCTION

The interaction of an aircraft gear with the pavement is dynamic, thus the load transferred by the wheels is different from the static loads reported in the aircraft specifications, and it is usually higher. The static can be calculated knowing the total weight of the aircraft and its gear configuration. The dynamic component of wheel induced loads depends on the road pavement profile and the functional characteristics of the vehicle (geometry, mass and stiffness distribution, tire and suspension type, operative speed, etc.).

The dynamic actions can be even higher and produce a general decay of the pavement or local breaks near the biggest pavement unevenness or near the Portland concrete cement (PCC) joints.

In a Cement Concrete pavement (rigid pavement) the adjacent slabs can be connected with steel bars (dowels): the dowels are installed across joints as load-transfer devices, leaving the joint the possibility to open and close allowing thermal expansion and contraction of the concrete. Several methods of theoretical analysis have been proposed to design these elements; most of them give dowel sizes and spacing that grant satisfactory service: surveys of existing pavements and extensive tests on full-scale slabs didn't show any clear case of dowel failure where the pavement slabs is adequate for the loads carried, according to these theories.

The load is transferred by the dowel through shear action, and results in reducing the deflection in the loaded slab and in giving a better distribution of stresses to the foundation. This rises the lifetime of the whole pavement system, since both the slab and the foundation are subjected to lower demands.

3D FINITE ELEMENT MODEL

The construction of the 3D Finite Element Model has been divided in two principal steps: the pavement and the aircraft gear.

Pavement

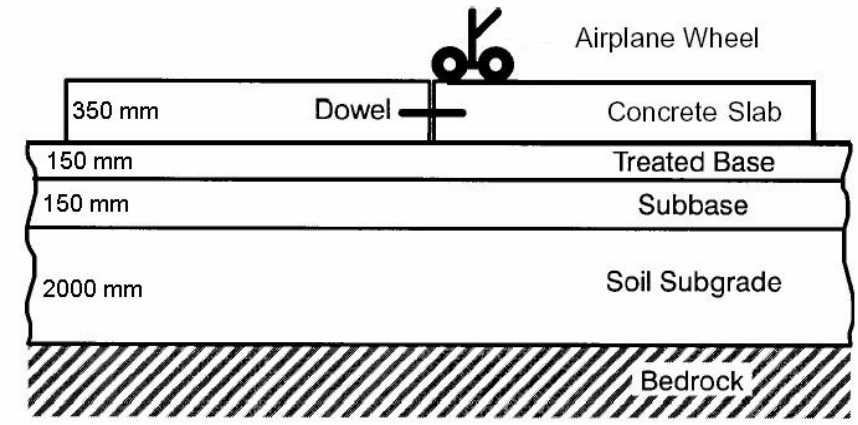

Figure 1 - Cross section of rigid pavement system

This layout, with the bedrock and these thicknesses, is a reproduction of a particular situation: different configurations could be easily analyzed modifying the geometry, material properties and boundary conditions of the model components. The model reproduces two full slabs, jointed with and without steel dowels; the slab dimensions are 3000x3600 mm; the whole model dimensions are shown in Figure 3.

LAYER	Young Modulus (MPa)	Poisson's ratio
Concrete Slab	30000	0.15
Treated base	5000	0.20
Subbase	500	0.35
Soil subgrade	200	0.50

Table 1 – Material properties of the pavement layers

In the following figures (Figure 2 and Figure 3) are reported a detailed view of the dowel joint system and the complete model of the pavement, with dimensions for each part.

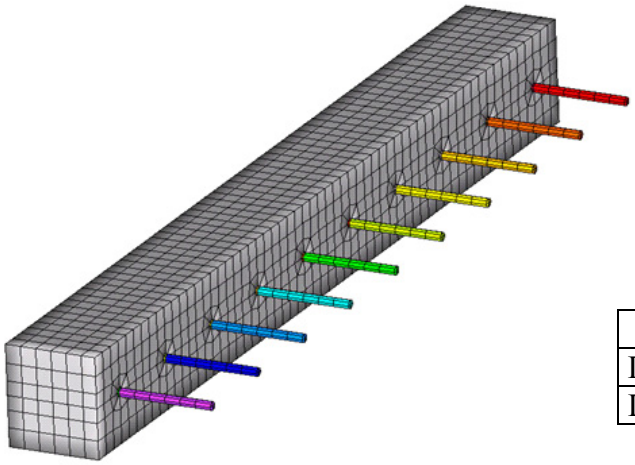

Dowel bar characteristics)	
Diameter	30 mm
Length	600 mm

Figure 2 - Detailed view of dowel joint system

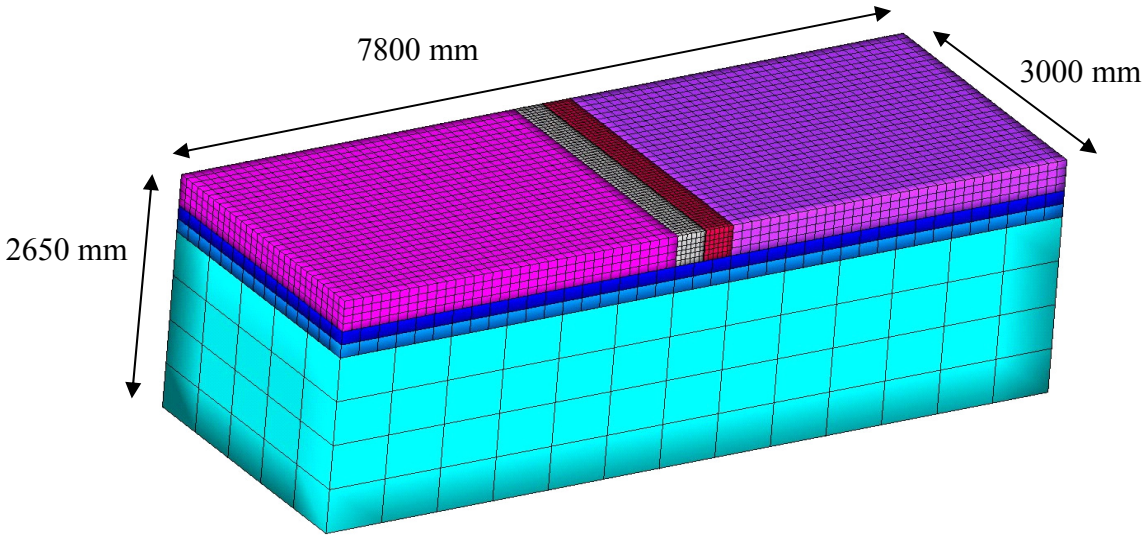

Figure 3 - Complete pavement model

The region close to the joint needed a particular attention during the development phase, since it is the zone where there is major interaction and stress concentration. It was necessary to change several times the mesh and the contact interface between concrete slab and dowel bars.

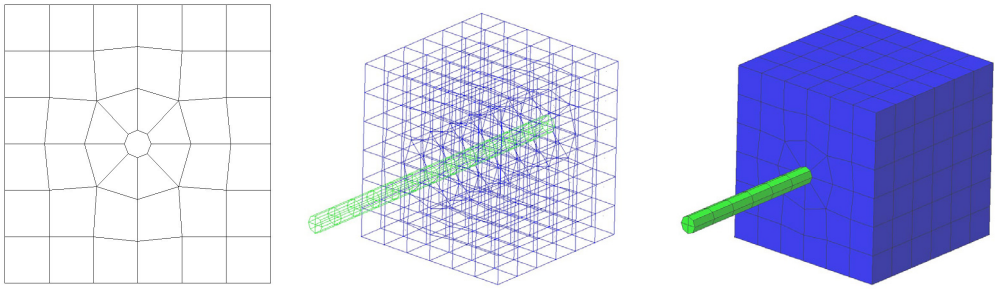

Figure 4 - Geometry free hand sketch and extruded elements

The final design is shown in Figure 4c: the construction started from a free hand sketch of the 2D mesh pattern (Figure 4a), subsequently reproduced through CAD program and imported in the Altair Hypermesh[5] preprocessor (Figure 4b). In this program, the command "3D extrude" was capable of creating a 3D Finite Element mesh, starting from the 2D input. Through "mirror" and "copy" commands, the part near the joint, was completed. After that, the concrete slabs and the subbase layers were completed, using 8 node solid element, that go in size according to depth.

The total number of elements used for the pavement is briefly reported in the next table 1:

ELEMENTS USED FOR THE PAVEMENT	
CONCRETE SLAB	
More defined part near the joint	4800 elements
Less defined part	8640 elements
Dowels	480 elements
CEMENT TREATED LAYER	585 elements
GRANULAR LAYER	585 elements
SUBGRADE	260 elements
TOTAL	**15350 elements**

Table 2 - Elements used for the pavement

Aircraft gear

The reference aircraft selected for this study is the Airbus A300; one of the aircraft gears has been modeled, trying to reproduce all the geometric and physic characteristics.

[5] Altair Hypermesh v.5.0, 2001, Altair Engineering, Inc.; http://www.altair.com/

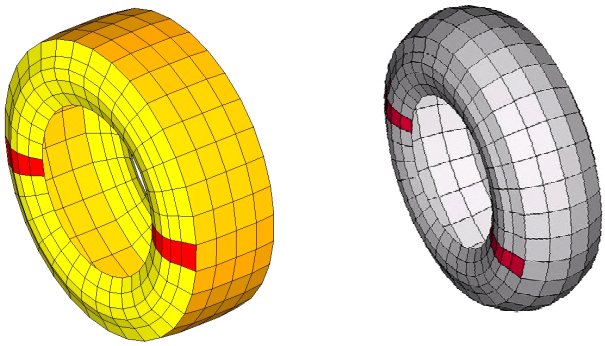

Figure 5 - Tire modeling

The main structure of the gear is built with shell elements; suspensions have been added to give a realistic load transmission between gear and pavement. The best way to do it, is to set a spring in parallel to a damper between chassis and bolt. The suspension mechanism is constituted by a superior triangle and a lower rectangle made with beam elements, connected by a vertical tie rod; the wheel axle is jointed to this latter vertical element. All these elements are connected with cylindrical joints, to make the wheels roll over the pavement surface. This is very important to study the wheel/pavement interaction, in particular in the landing zones (not analyzed in this paper).

After that, tires have been modeled: starting from a truck tire, used for numerical analysis for standard road pavements, it has been remodeled to give it a shape, the characteristics and a behavior of an aircraft tire (Figure 5).

The last step was to put the load, modeled with the mass of hi-density solid elements. The final model of the aircraft gear is presented in the next Figure 6.

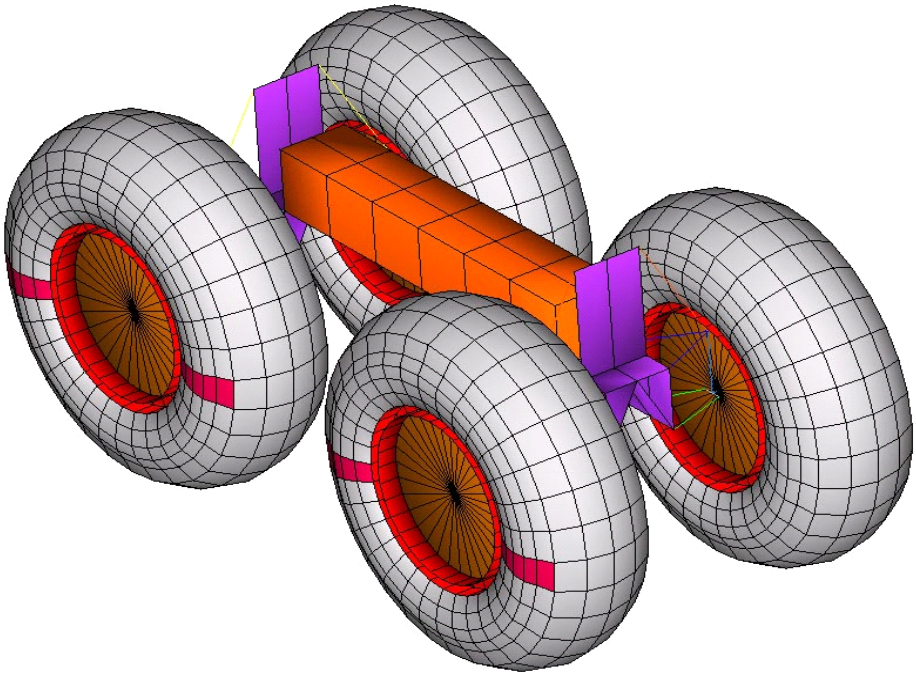

Figure 6 - Complete model of the aircraft gear

The total number of elements used for the aircraft gear is briefly reported in the next table (Table 3).

ELEMENTS USED FOR THE AIRCRAFT GEAR	
CHASSIS	40 shell elements
SUSPENSIONS	60 beam and discrete elements
LOAD	12 solid elements
TIRES	
Tire tread	512 shell elements
Tire side	1280 shell elements
Tire rim	1408 shell elements
TOTAL	**3312 elements**

Table 3 Elements used for the aircraft gear

Boundary conditions and contact interfaces

The nodes along the lateral surfaces are not constrained to simulate the behavior of these small size slabs, without lateral interaction with other elements; again, it is possible to choose a different layout for the pavement and modify the model to study the different situation. Nodes on the lower base (set 2.65 m depth) are fully constrained.

It has been necessary to use a special contact type to join and keep together the two parts of the concrete slab (the more detailed with holes for dowels, and the less detailed),.

Ideally (Hallquist,1998), each master node should coincide with a slave node to ensure complete displacement compatibility along the interface, but in practice this is often difficult if not impossible to achieve. In other words, master nodes that do not coincide with a slave node can interpenetrate through the slave surface.

Implementation of tied interface (Figure 7) constraints is straightforward. Each time step, the program, loop through the tied interfaces and update each one independently. First, it distributes the nodal forces and nodal mass of each slave node to the master nodes which define the segment containing the contact point. After this, it can compute the acceleration of the master surface.

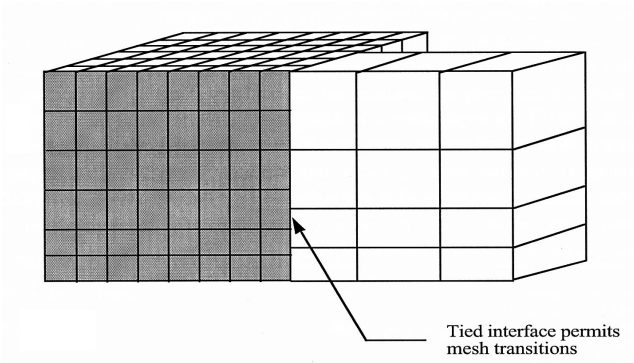

Figure 7 - Tied interface

This contact type has been also used to model the interface between the concrete slab and the dowels in one side of the joint (the fixed one).

All the other contact types are “automatic contacts”. Through the definition of the frictional coefficient and the two parts, the code automatically checks the penetration between every element in the two parts and adjusts the element surface normals.

The complete model, shown in the following figure (Figure 8), through the modification of some parameters (aircraft speed and discontinuities between slabs), permitted to obtain significant results for our study. Next, a table is reported, containing the total number of elements used for the complete model (Table 3).

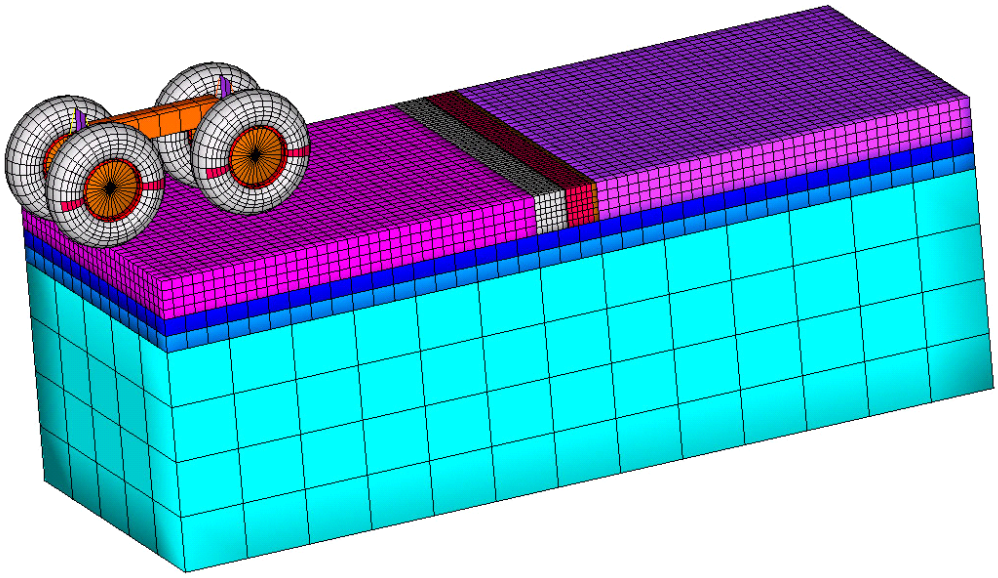

Figure 8 - Complete model of the aircraft gear on the pavement test area

ELEMENTS USED FOR THE COMPLETE MODEL	
Pavement	15350 elements
Aircraft gear	3312 elements
TOTAL	***18662 elements***

Table 4 Total number of elements used for the complete model

PARAMETRIC STUDY: RESULT

We have chosen to make a parametric study to understand the airport pavement behavior under dynamic loads, caused by aircraft traffic.

The parameters selected for our study were: the aircraft speed (from 5 m/s to 20 m/s) and the bump height between slabs (form 0 cm to 3 cm).

The code used to perform all the analysis was LS-DYNA v.950d[6], a nonlinear explicit Finite Element Analysis code built on the basis of DYNA-3D code, initially developed in the Lawrence Livermore National Laboratory[7].

---

[6] Livermore Software Technology Corporation, 2001, http://www.lstc.com/
[7] http://www.llnl.gov/eng/mdg/Codes/body_codes.html

Tensile stress at the base of the slab

The first results are the tensile stresses at the base of the slab. The time step chosen to represent the stress condition of the entire system is the one when the aircraft gear is completely over the second slab. This has been made to have our conditions more similar to the Westergaard "edge" load conditions, with which, later, we made a comparison.

To do this, we used a different model without the dowels; in the next figure (Figure 9) it's possible to see the stress distribution in the slab, near the joint (σ_{yy} stress in our coordinate system).

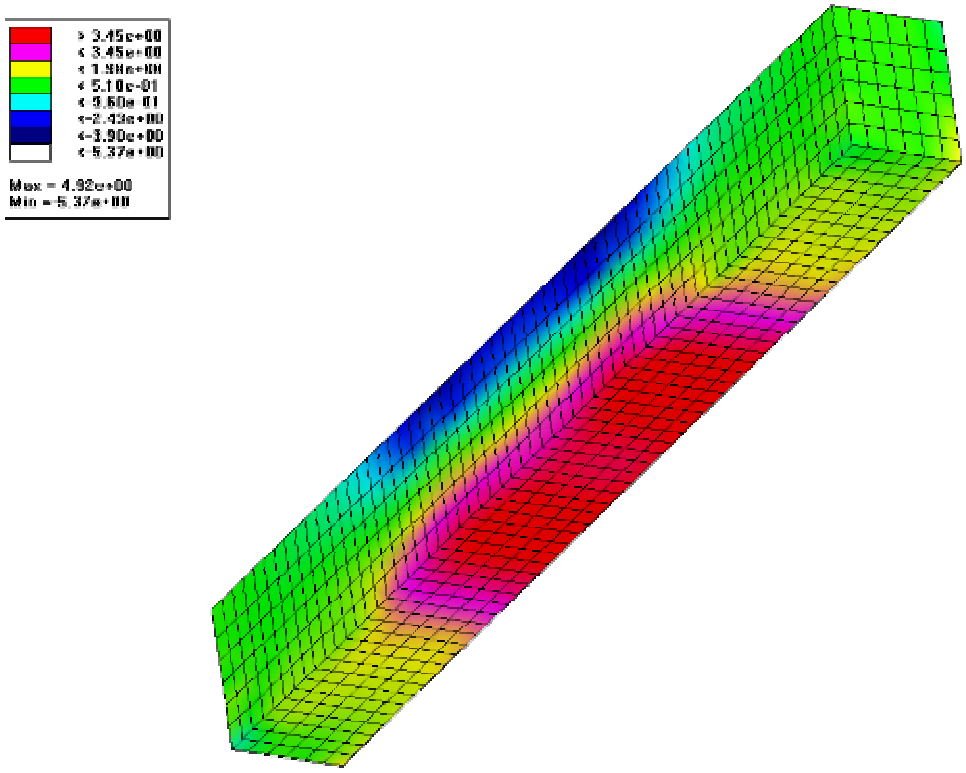

Figure 9 - Stress distribution in the slab

Here are the table of results (Table 5) and the graphic (Figure 10) of the tensile stress.

TENSILE STRESS (Kg/cm^2)				
	0 cm	***1 cm***	***2 cm***	***3 cm***
5 m/s	32.98	33.27	34.92	35.98
10 m/s	32.49	35.12	37.64	39.34
15 m/s	32.46	37.81	40.82	43.95
20 m/s	32.37	40.49	45.87	51.86

Table 5 Tensile stress in the slab

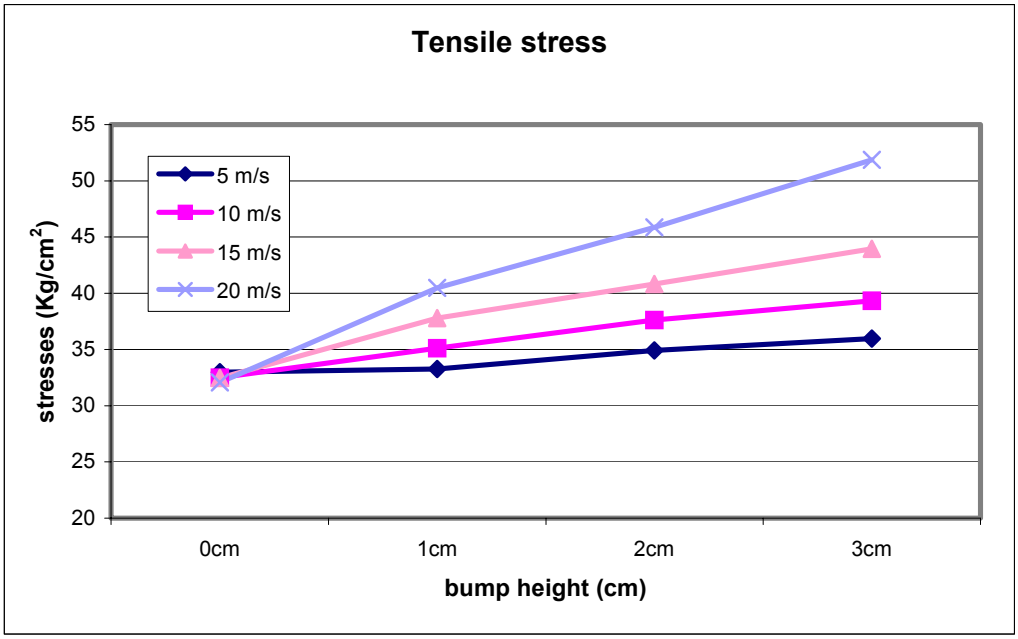

Figure 10 - Graphic of the tensile stress in the slab

Comparison between our result and Westergaard analysis

Using the edge load formula by Westergaard, we calculated the maximum tensile stress in the static condition. For this, we considered the presence of dual wheels through the Equivalent Single Wheel Load (ESWL) transformation formula.

We have found:

$$ESWL = \frac{2 \cdot 16250}{1.45} = 22413Kg\,.$$

Therefore, the maximum tensile stress for Westergaard is:

$$\sigma_b = 0.529 \cdot (1 + 0.54\mu)\frac{P}{h^2}\left[4\log\left(\frac{l}{b}\right) + 0.359\right] = 29.63Kg/cm^2\,.$$

At this point, we made a 3-dimensional graphic (Figure 11) with the quadratic regression method, and we obtained a 3D surface that represents clearly the stress trend in various condition. The violet plane is the Westergaard static stress plane.

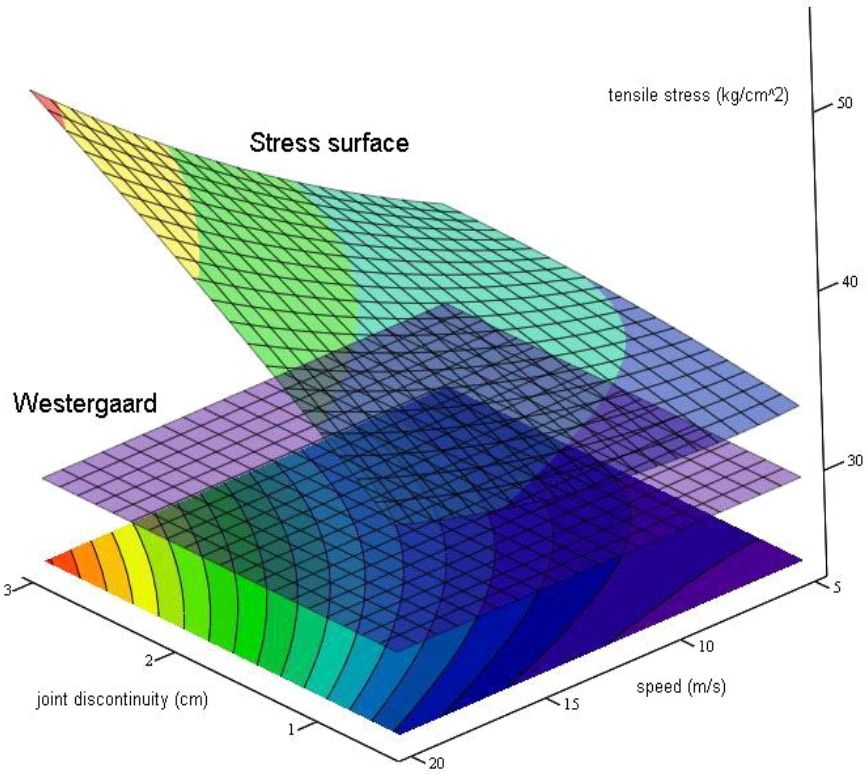

Figure 11 - 3D stress surface

The graphic was also projected in the plane for a more clear reading (Figure 12).

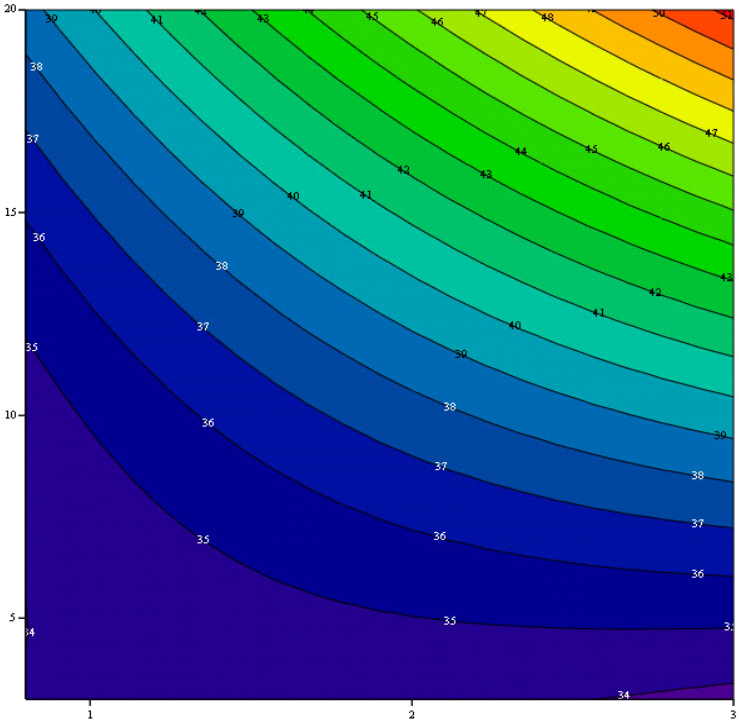

Figure 12 – 2D projection of the stress surface

After this result, we tried to make a reciprocal analysis. Starting from our model stress, we back-calculated the real single wheel load corresponding to a defined stress condition; in this way we have been able to define some coefficients; multiplying the starting load with these coefficient, it's possible to find a "dynamic equivalent load" for each stress condition.

Using a symbolic mathematics computer code and some iterative calculus, we solved the formula presented below (Figure 13). The equivalent single wheel loads are reported in the next Table 6.

$$\sigma b = 0.529 \cdot (1 + 0.54 \cdot \mu) \cdot \left[\frac{(2Pr)}{h^2} \right] \cdot \left[4 \log \left[\frac{l}{\sqrt{1.6 \cdot \frac{p}{\pi} + h^2} - 0.675 \cdot h} \right] + 0.359 \right]$$

Figure 13 - Formula used to calculate the equivalent single wheel loads

SINGLE WHEEL EQUIVALENT LOADS				
	0 cm	**1 cm**	**2 cm**	**3 cm**
5 m/s	18668	18886	20151	20988
10 m/s	18303	20307	22341	23782
15 m/s	18281	22483	25086	28009
20 m/s	18215	24792	29924	36603

Table 6 - Single wheel equivalent loads

After that, the loads has been divided by the starting load (16250 Kg) (Table 7) and in this way, we have found the amplification load coefficients (Figure 14).

AMPLIFICATION COEFFICIENTS				
	0 cm	**1 cm**	**2 cm**	**3 cm**
5 m/s	1.15	1.16	1.24	1.29
10 m/s	1.13	1.25	1.37	1.46
15 m/s	1.12	1.38	1.54	1.72
20 m/s	1.12	1.53	1.84	2.25

Table 7 - Amplification coefficients

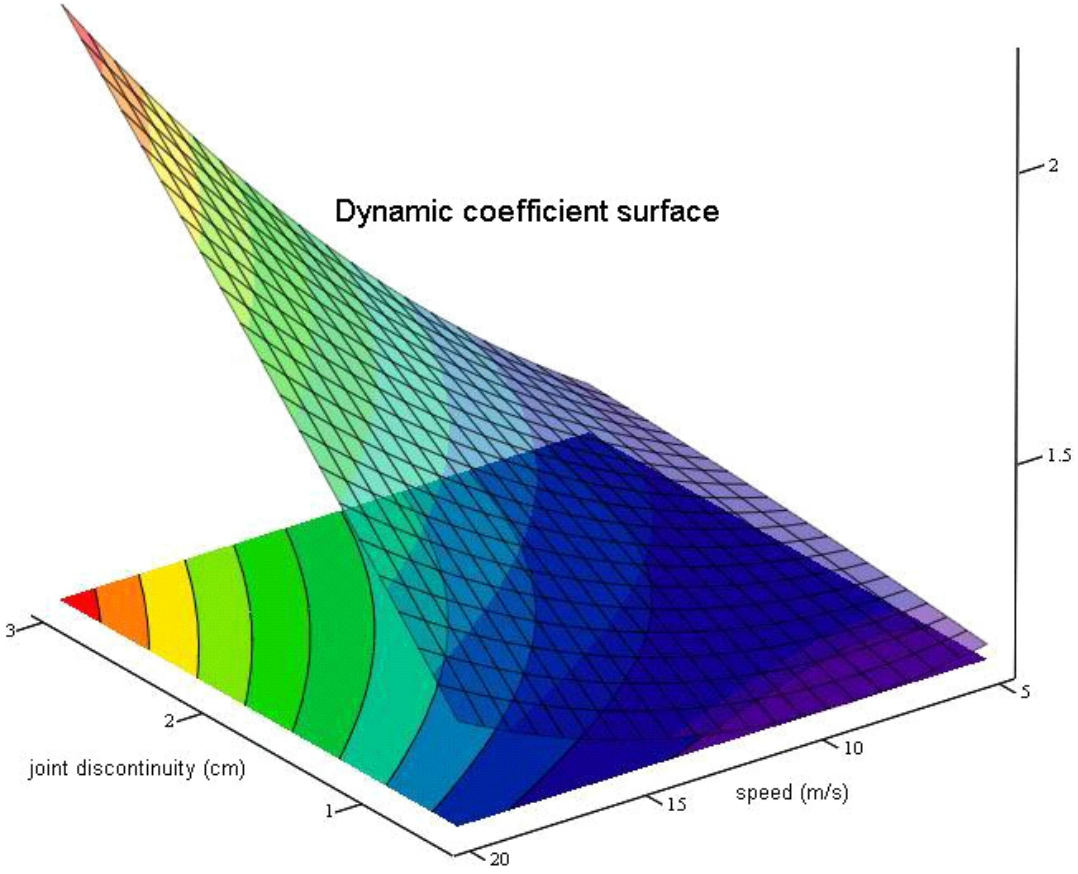

Figure 14 – 3D surface of dynamic coefficients

Dowels efficiency

To evaluate the load transfer capacity of dowel bars (Figure 15), for the various aircraft speeds and joint bump heights, we compared the deflection of a set of nodes in the loaded slab and the corresponding nodes on the unloaded slab, in the same time step.

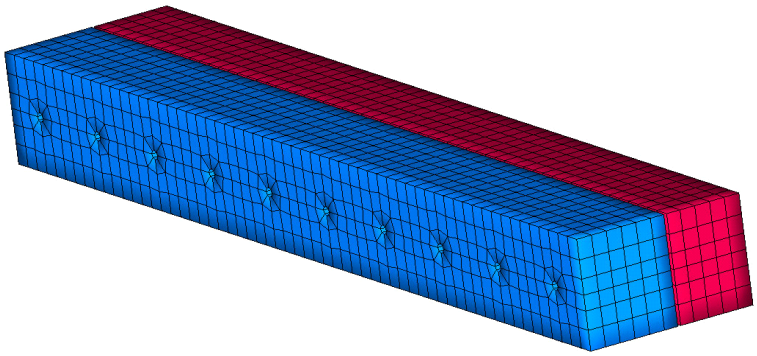

Figure 15 - Rigid pavement joint

Deflection load transfer efficiency (LTE_δ) is defined [Hammonds and Ioannides,1992] as the ratio of the deflection of the unloaded slab to the deflection of the loaded slab, as follows:

$$LTE_\delta = \frac{\Delta_U}{\Delta_L}.$$

Results are reported as percentage, in the following table (Table 7), and represented as a tri dimensional surface in Figure 16:

LTE_δ LOAD TRANSFER EFFICIENCY				
	0 cm	**1 cm**	**2 cm**	**3 cm**
5 m/s	89%	82%	77%	74%
10 m/s	87%	76%	74%	68%
15 m/s	85%	74%	71%	70%
20 m/s	82%	73%	70%	69%

Table 8 - Load transfer efficiency

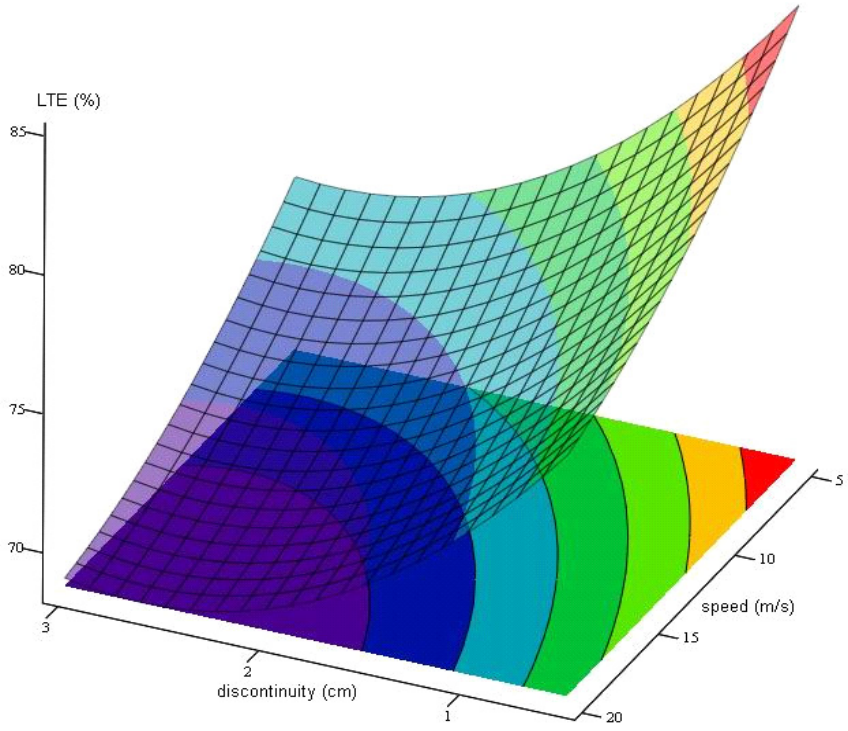

Figure 16 - LTE surface

CONCLUSIONS

A 3D finite element model that simulates the interaction between an aircraft gear and a rigid pavement has been developed. This model permits to determinate the maximum stress in the slab, due to dynamic loads, changing the different parameters of the model (masses, materials, constitutive laws, operative aircraft gear parameters).

Results of this parametric study, obtained with different aircraft speeds and different bump heights, showed the following aspects:

1. the stresses increase, caused by dynamic loads, cannot be neglected when joint discontinuities are present, also for normal speeds. For example, a joint discontinuity (1 cm high), at 10 m/s (taxi-way speed), increments the static stress up to 20 percent. At the same speed, with a 2 cm bump, the stress can be up to 40 percent higher.

2. Raising the dynamic load, the dowel transfer capacity is reduced.

However, it must be noted that the analyses conducted here are by no means comprehensive, and the issue of dowel/slab interaction under dynamic loads deserve further investigation, both simulation-based and experimental.

A full scale test should be performed to validate the model in real condition, and to deeply understand the rigid pavement system behavior.

REFERENCES

[1] M. I. Hammons, A. M. Ioannides. Mechanistic design and analysis procedure for doweled joints in concrete pavements, Proceedings, Sixth International Conference on Concrete Pavement Design and Rehabilitation, Purdue University, Indianapolis, IN (Nov., 18-21, 1997), pp.221-223.

[2] D. Parsons, I. S. Eom, K. D. Hjelmstad. Numerical simulation of load transfer between doweled pavement slabs, Proceedings, Sixth International Conference on Concrete Pavement Design and Rehabilitation, Purdue University, Indianapolis, IN (Nov., 18-21, 1997), pp 166-169.

[3] J. Kim, K. Hjelmstad. Three dimensional finite element analysis of multilayered system: Compressive nonlinear analysis of rigid airport pavement system (1990), Center of Excellence for airport pavement research COE Report N.10.

[4] L. Domenichini. Pavimentazioni stradali in calcestruzzo, Associazione italiana tecnico economica del cemento.

[5] F.M. Fiordoliva, Analisi e modellazione numerica delle azioni dinamiche da traffico su pavimentazioni in calcestruzzo, Tesi di laurea, Università degli studi di Roma “La Sapienza”, 2001.

[6] V. Grilli, N. Di Matteo. Le pavimentazioni cementizie per piste e piazzali di aeroporti.

[7] A. Maschiella. Irregolarità superficiali delle pavimentazioni stradali: calcolo delle interazioni dinamiche conseguenti, Tesi di laurea, Università degli studi di Roma “La Sapienza”, 2001.

[8] R. G. Packard. Design of concrete airport pavement, Portland cement association.

[9] AASHTO (1993). AASHTO Guide for the design of pavement structures.

[10] W. G. Davids. 3D Finite element study on load transfer at doweled joints in flat and curled rigid pavements, Second International Symposium on 3D Finite Element for Pavement Analysis, design and research, Charleston (West Virginia), October 11-13, 2000.

[11] G. W. William, S. N. Shoukry. 3D Finite element analysis of temperature-induced stresses in dowel jointed concrete pavements, Second International Symposium on 3D Finite Element for Pavement Analysis, design and research, Charleston (West Virginia), October 11-13, 2000.

[12] M. Ioannides, G. T. Korovesis. Analysis and design of doweled slab-on-grade pavement system, Journal of transportation engineering, pp. 745-768.

[13] Y. Huang. Pavement analysis and design, Prentice-Hall, Englewood Cliffs, NJ, 1993.

[14] Federal Aviation Administration, Office of airport safety and standards. Airport Pavement design and evaluation, Advisory circular AC 150/5320-16, 1995.

[15] D. R. Brill, X. Lee. Three dimensional finite element modeling of Portland cement concrete airport pavements part II: Finite element prediction vs. field-measured data, Proceedings of the FAA Worldwide airport technology transfer conference, Atlantic City, New Jersey, American Association of Airport Executives, April 1999.

[16] D. R. Brill, X. Lee. Stress analysis of concrete airport pavement with high stiffness base layer, in Modeling and simulation based engineering, S.N. Alturi and P. E. O'Donoghue, editors, Tech Science Press, 1998 pp. 1665-1670.

[17] R. G. Ahlvin, H. H. Ulery, R. L. Hutchinson, J. L. Rice. Multiple-wheel heavy gear load pavement tests, volume 1 – Basic report, Technical report S-71-17, US Army Engineer Waterways Experiment Station, Vicksburg, Mississippi, November 1971.

[18] J. O. Hallquist. LS-DYNA Theoretical manual (1998),Livermore software technology corporation,pp.23.21-23.22, 1998.

[19] D. Cebon. Handbook of Vehicle-Road Interaction, Swets and Zeitlinger B.V., Lisse, the Netherlands, (1999).

[20] Ranzo, P. Di Mascio, G. Loprencipe. Bridge joint as pavement surface unevenness., 5th World Congress on Joints, Bearings and Seismic Systems for Concrete Structures - Rome, Italy 7-11 October 2001.